Broadband solid cloak for underwater acoustics

Yi Chen[1], Mingye Zheng[1], Xiaoning Liu[1†], Yafeng Bi[2], Zhaoyong Sun[2], Ping Xiang[3], Jun Yang[2], Gengkai Hu[1†]

[1]*Key Laboratory of Dynamics and Control of Flight Vehicle, Ministry of Education, School of Aerospace Engineering, Beijing Institute of Technology, Beijing 100081, China*

[2]*Key Laboratory of Noise and Vibration Research, Institute of Acoustics, Chinese Academy of Sciences, Beijing 100190, China*

[3]*System Engineering Research Institute, Beijing 100094, China*

[†]Correspondence to: G. K. Hu (hugeng@bit.edu.cn) or X. N. Liu (liuxn@bit.edu.cn)

Abstract: Shielding an object to be undetectable is an important issue for engineering applications. Cloaking is the ultimate shielding example, routing waves around an object without mutual interaction, demonstrated as possible in principle by transformation and metamaterial techniques. Example applications have been successfully designed and validated for electromagnetic wave, thin plate flexural wave, thermal flux, and airborne sound. However, for underwater acoustics, the commonly used scheme based on meta-fluids with anisotropic density for airborne sound is unworkable since an acoustic rigid material is required with mass density three orders of magnitude higher than water. Material with such high density is impossible using even the heaviest metal, and may suffer from a narrow working frequency band even if realized with locally resonant techniques. In any case, such cloak would be inherently fluid with only limited practical interest. An alternative solution was recently suggested based on solid pentamode material, which can be impedance matched with water and has anisotropic modulus. A cloak constructed from this material was theoretically shown to have broadband frequency range effect, and sufficient solidity to be potentially suitable for underwater applications. Here, we report an underwater solid cloak with broadband efficiency utilizing pentamode material machined from aluminum. The cloak was composed with a graded subwavelength scale microstructure to meet the required effective property designed by transformation method. Transient wave experiments conducted in a waveguide validate cloaking effectiveness: the underwater acoustic wave is guided around the cloaked object with substantial reduction of both scattering and shadow over a broad frequency range. This finding paves the way for controlling underwater acoustics using achievable and available metamaterials with broadband efficiency, and may stimulate development of new technologies, such as directed communications, advanced detection systems, or cloaking devices against underwater acoustics.

Cloaking as an ultimate shielding example, demonstrated as possible in principle by transformation[1,2] and metamaterial technique[3,4], has been successfully designed for different physical fields[5-20]. As for air-borne sound, acoustic ground cloaks have been experimentally demonstrated using perforated plates in air[16,17], which serves as the meta-fluid with anisotropic density. However, this material design scheme is unsuitable for dense fluids such as water due to the enormous material density required, preventing underwater acoustic cloaking from being realized. Solid material cloaking is highly desired, but the difficulty lies in different propagating velocities for longitudinal and shear waves coexistent in a solid, which are hard to control simultaneously. Tailoring the material deformation modes through microstructure design allows five easy deformation modes[21], enabling a single pseudo pressure wave. This pentamode (PM) material acts as a meta-fluid with anisotropic modulus realized by the micro structured solid[24-28]. PM material can be impedance matched with water and provide much larger achievable modulus anisotropy[26,27,29] than available through just density variations[16,17,30], offering unprecedented flexibility for underwater acoustic control. Underwater cloaks have been designed based on PM material using transformation approach[22,23], and shown to have broadband effects from a solid shield[27] which is particularly suitable for underwater applications[28].

However, experiment demonstration has not been reported due to lack of microstructure design and measurement systems for 2D underwater waveguide. This study reports an underwater solid cloak composed of five graded PM material layers. Transient wave experiments conducted in a specially designed 2D underwater waveguide validated superior

wave shielding performance of the designed cloak, with 6.3 dB average reduction of target strength achieved across a broad frequency band 9–15 kHz.

Figure 1a shows the fabricated cylindrical cloak, machined from aluminum block using advanced electrical discharge machining (EDM) technique with high accuracy. The fabricated cloak had inner diameter 200mm; outer diameter 334 mm; height 50 mm; and mass 4.87 kg, which is quite close to the mass of an ideal cloak (4.42 kg)[22]. The cloak consisted of 50 sectors of cells around the θ-direction, and a zoomed sector in Fig. 1b (bounded by red lines) shows five graded unit cells along the r direction. Calibrating six geometric parameters of the proposed unit cell (Fig. 1c), effective moduli, K_θ and K_r, and density, ρ, of each layer were tuned to provide the derived optimized material anisotropy and property gradient (Fig. 1d, 1e). Modulus anisotropy, K_θ/K_r, increases from outer to inner sides, reaching 40 for the first two layers, while the outermost layer is nearly impedance matched with water (Z_{cloak}/Z_{water}=0.94, Z represents impedance). A relatively thin cloaking shell and coarse layer optimized discretization is chosen to facilitate fabrication while still achieving broadband shielding performance due to the strong anisotropy of the proposed unit cell. (See Methods, Table S1, S2).

Since the size of the fabricated cloak in z-direction is small, due to fabrication limitations, it is necessary to make measurements in a 2D underwater waveguide. However, designing 2D underwater waveguides is not trivial, since the large water density excludes any solid plate of feasible thickness from serving as an acoustic rigid boundary. Therefore, we propose a 2D water waveguide based on pressure compensation (See Methods). The waveguide was

composed of two opposing aluminum plates and a cylindrical piezoelectric transducer (PZT) immersed in an anechoic water pool (Fig. 2a). The cloak and scatter were mounted in the middle of the waveguide chamber. The voids in the cloaking shell must be free of water, so the top and bottom cloak surfaces were sealed with 4 mm thick water matched rubber. A thin walled polymethyl methacrylate (PMMA) hollow cylinder (diameter 200 mm and height 50 mm) was used as the scatter, which can be treated as air scatter with extremely small density.

To test broadband performance, it is preferable to use transient rather than steady waves of a single frequency. We adopted a Gaussian burst of form $\exp(-0.222(f_c t)^2)\cos(2\pi f_c t)$ to drive the PZT, where f_c denotes the central frequency. Figure 2b shows the driven signal for f_c=13 kHz, which lasts 0.7ms to distinguish between incident and reflective signals. At this central frequency, one wavelength is approximately 11 largest unit cells of the cloak, so the homogenization condition holds. The frequency transformed signal (Fig. 2c) spans from 10–16 kHz with amplitude larger than 10% of the central frequency amplitude, hence broadband performance of the cloak can be verified. In the experiment, acoustic pressure fields corresponding to forward and backward regions (Fig. 2a) inside the waveguide for three cases: reference (empty waveguide), uncloaked scatter, and cloaked scatter, were scanned using a hydrophone moving along orthogonal axes with 10 mm step (See Methods, Fig. S1). Transient wave numerical simulations are performed to validate the proposed underwater waveguide as well as the designed cloak (Fig. S2–S4).

Figures 3a–3c show snapshots of pressure fields in the forward region. For the reference case (Fig. 3b), pressure fields show nearly undisturbed cylindrical wave form as expected, and this provides a measurement benchmark. Small distortion in the wave front stems from interference with the reflected wave from the edge of the waveguide owing to the small impedance mismatch between waveguide chamber and outside free space, which was also observed in numerical simulations (Fig. S2). For the uncloaked scatter case (Fig. 3c), the impinging cylindrical wave burst is mostly blocked due to significant impedance mismatch with water, and a clear shadow is formed behind the scatter. A small amount of energy flows around the scatter from the lateral side, inducing phase lag owing to the longer propagation trajectory. When the scatter is covered with the cloak (Fig. 3a), impinging acoustic energy is almost completely transformed into an elastic wave at the solid/fluid interface and directed by the designed graded material properties towards the forward region, substantially eliminating the acoustic shadow behind the scatter and restoring the pressure field to the reference case (Fig. 3b). Pressure along the indicated horizontal line in the forward region is shown for the three cases (Fig. 3g). The pressure distributions are very similar for the empty waveguide and cloaked scatter in contrast to the uncloaked scatter.

Figures 3d-3e show pressure in the backward region when the incident wave has been totally reflected. The reflected wave is only clearly observed for the uncloaked case. The cloaked case shows much less reflection (Fig. 3d) and absolute pressure along the indicated line remains the same level as the reference case (Fig. 3h). These results validate the impedance match of the cloak with water, and also indicate excellent cloaking effect for the

enclosed scatter. Videos showing wave propagation in the forward and backward regions are provided in Supplemental Information (MOV.S1). A further experiment investigating scattering of an aluminum cylinder also verified the designed waveguide. (Fig. S4, MOV.S5).

Figures 4a–4d show the pressures measured at locations 1–4 in Fig. 2a, respectively. At backward location 1 (Fig. 4a), the incident Gaussian packet for all three cases are similar, whereas the reflected Gaussian packet immediately following the incident packet is only clearly seen for the uncloaked case. The reflected and incident signal partly overlap due to the large water wave velocity, and is significantly reduced when cloaked. This suppressing effect for the reflected signal is more clearly identified at another backward location (Fig. 4b). Forward location 3 (Fig. 4c) shows weaker and phase retarded signals compared to reference case for uncloaked scatter, whereas cloaked, phase retardation is rectified with moderate amplitude recovery. The other forward location 4 (Fig. 4d) shows both amplitude and phase lag were perfectly restored with the cloak.

Finally, we quantified the broadband efficiency of the designed cloak using target strength reduction (TSR), calculated from the reflective signal strength. The TSR with covered cloak can be obtained as $10\times\mathrm{Log}_{10}(E_{\mathrm{cl}}/E_{\mathrm{un}})$, where E_{cl} and E_{un} represent the reflective signal energy for the uncloaked and cloaked case, respectively, at the same backward location. Additional experiments using signals with different central frequencies were conducted to cover a wide frequency band (see Methods, MOV.S2–S4). The measured signal was taken from location 2 rather than 1 to calculate TSR with clearly distinguished reflected and incident signals. In the studied frequency range, simulated TSR (Fig. 4e) is nearly constant

with small peaks caused by shear resonance scattering[27]. The overall trend of measured TSR is consistent with simulation, where differences may arise from system errors including fabrication, measurement, and imperfect waveguide. The experiment validates superior stealth capability of designed cloak, achieving 6.3 dB average reduction within a remarkably broad frequency range 9–15 kHz. It should be noted, although measurements here only indicate the excellent performance of the designed cloak over the given range owing to transducer frequency limitations, the designed cloak can in principle work from zero frequency, since only quasi-static material properties are employed, in contrast to inertial cloaks based on local resonance mechanisms.

We have experimentally demonstrated a broadband solid cloak for underwater acoustics. The cloak is composed of graded pentamode unit cells with varying anisotropic modulus for bending underwater acoustic waves around covered object, which is impossible with conventional meta-fluids of anisotropic density. Solid and broadband features of pentamode materials offer new possibility to control underwater acoustic waves with unprecedented flexibility. Many applications for underwater acoustic may arise from this concept, such as acoustic radiation shaping, elastic/acoustic energy transforming device, etc.

Supplementary materials:

Methods
Tables S1–S2
Figures S1–S4
Movies S1–S4

References

1. Pendry, J. B., Schurig, D. & Smith, D. R. Controlling electromagnetic fields. *Science* **312**, 1780-1782 (2006).
2. Leonhardt, U. Optical conformal mapping. *Science* **312**, 1777-1780 (2006).
3. Smith, D. R. *et al.* Composite medium with simultaneously negative permeability and permittivity. *Phys. Rev. Lett.* **84**, 4184-4187 (2000).
4. Liu, Z. *et al.* Locally resonant sonic materials. *Science* **289**, 1734-1736 (2000).
5. Schurig, D. *et al.* Metamaterial electromagnetic cloak at microwave frequencies. *Science* **314**, 977-980 (2006).
6. Cai, W., Chettiar, U. K., Kildishev, A. V. & Shalaev, V. M. Optical cloaking with metamaterials. *Nat. Photonics* **1**, 224-227 (2007).
7. Edwards, B., Alù, A., Silveirinha, M. G. & Engheta, N. Experimental verification of plasmonic cloaking at microwave frequencies with metamaterials. *Phys. Rev. Lett.* **103**, 153901 (2009).
8. Valentine, J. *et al.* An optical cloak made of dielectrics. *Nat. Mater.* **8**, 568-571 (2009).
9. Liu, R. *et al.* Broadband ground-plane cloak. *Science* **323**, 366-369 (2009).
10. Zhang, B., Luo, Y., Liu, X. & Barbastathis, G. Macroscopic invisibility cloak for visible light. *Phys. Rev. Lett.* **106**, 33901 (2011).
11. Landy, N. & Smith, D. R. A full-parameter unidirectional metamaterial cloak for microwaves. *Nat. Mater.* **12**, 25-28 (2013).
12. Stenger, N., Wilhelm, M. & Wegener, M. Experiments on Elastic Cloaking in Thin Plates. *Phys. Rev. Lett.* **108** (2012).
13. Misseroni, D. *et al.* Cymatics for the cloaking of flexural vibrations in a structured plate. *Sci. Rep.* **6**, 23929 (2016).
14. Xu, H. *et al.* Ultrathin Three-Dimensional thermal cloak. *Phys. Rev. Lett.* **112**, 54301 (2014).
15. Han, T. *et al.* Experimental demonstration of a bilayer thermal cloak. *Phys. Rev. Lett.* **112** (2014).
16. Zigoneanu, L., Popa, B. & Cummer, S. A. Three-dimensional broadband omnidirectional acoustic ground cloak. *Nat. Mater.* **13**, 352-355 (2014).
17. Popa, B., Zigoneanu, L. & Cummer, S. A. Experimental acoustic ground cloak in air. *Phys. Rev. Lett.* **106**, 253901 (2011).
18. Cummer, S. A. & Schurig, D. One path to acoustic cloaking. *New J. Phys.* **9**, 45 (2007).
19. Chen, H. & Chan, C. Acoustic cloaking in three dimensions using acoustic metamaterials. *Appl. Phys. Lett.* **91**, 183518 (2007).
20. Zhang, S., Xia, C. & Fang, N. Broadband acoustic cloak for ultrasound waves. *Phys. Rev. Lett.* **106**, 24301 (2011).
21. Milton, G. W. & Cherkaev, A. V. Which elasticity tensors are realizable? *J. Eng. Mater-T. Asme* **117**, 483-493 (1995).
22. Norris, A. N. Acoustic cloaking theory. *P. Roy. Soc. A-Math. Phy.* **464**, 2411-2434 (2008).
23. Scandrett, C. L., Boisvert, J. E. & Howarth, T. R. Acoustic cloaking using layered pentamode materials. *J. Acoust. Soc. Am.* **127**, 2856-2864 (2010).
24. Kadic, M. *et al.* On the practicability of pentamode mechanical metamaterials. *Appl. Phys. Lett.* **100**, 191901 (2012).
25. Bückmann, T. *et al.* An elasto-mechanical unfeelability cloak made of pentamode metamaterials. *Nat. Commun.* **5** (2014).
26. Layman, C. N. *et al.* Highly anisotropic elements for acoustic pentamode applications. *Phys. Rev. Lett.* **111**, 24302 (2013).
27. Chen, Y., Liu, X. & Hu, G. Latticed pentamode acoustic cloak. *Sci. Rep.* **5**, 15745 (2015).
28. Hladky-Hennion, A. C. *et al.* Negative refraction of acoustic waves using a foam-like metallic structure. *Appl. Phys. Lett.* **102**, 144103 (2013).
29. Kadic, M., Bückmann, T., Schittny, R. & Wegener, M. On anisotropic versions of three-dimensional pentamode

metamaterials. *New J. Phys.* **15** (2013).

30. Torrent, D. & Sanchez-Dehesa, J. Anisotropic mass density by radially periodic fluid structures. *Phys. Rev. Lett.* **105**, 430117 (2010).

Acknowledgements

We acknowledge funding support from the Natural Science Foundation (Grant No. 11472044, 11221202, 11632003, 11521062) and from 111 Project (B16003). The authors would like to thank H. Jia for discussion on waveguide design, and X. Ruan for preparing part of hardware devices.

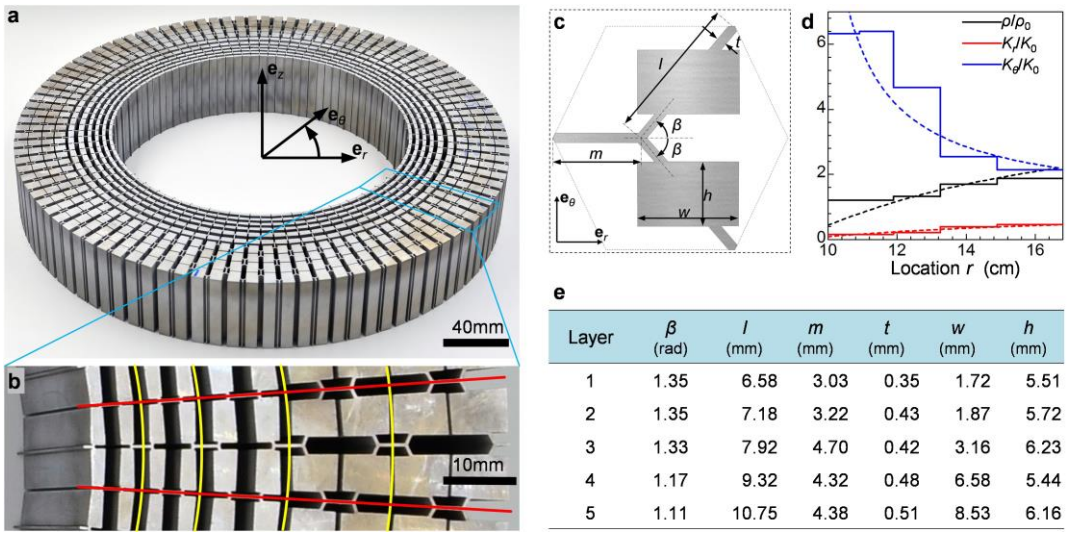

e

Layer	β (rad)	l (mm)	m (mm)	t (mm)	w (mm)	h (mm)
1	1.35	6.58	3.03	0.35	1.72	5.51
2	1.35	7.18	3.22	0.43	1.87	5.72
3	1.33	7.92	4.70	0.42	3.16	6.23
4	1.17	9.32	4.32	0.48	6.58	5.44
5	1.11	10.75	4.38	0.51	8.53	6.16

Figure 1 | Solid cloak designed from pentamode material. **a,** Image of the cloak machined from an aluminum block, consisting of 500 hexagonal unit cells. **b,** Enlarged view of one segment, highlighted in **a**. Structure between red lines represents one sector in the θ-direction and yellow lines separate the five graded unit cells. **c,** Proposed pentamode unit cell with six geometric parameters for tuning effective material properties. **d,** Homogenized density and in-plane moduli, normalized by water, of the designed cloak. Dashed lines represent properties derived from transformation. **e**, Geometric parameters corresponding to the five graded unit cells.

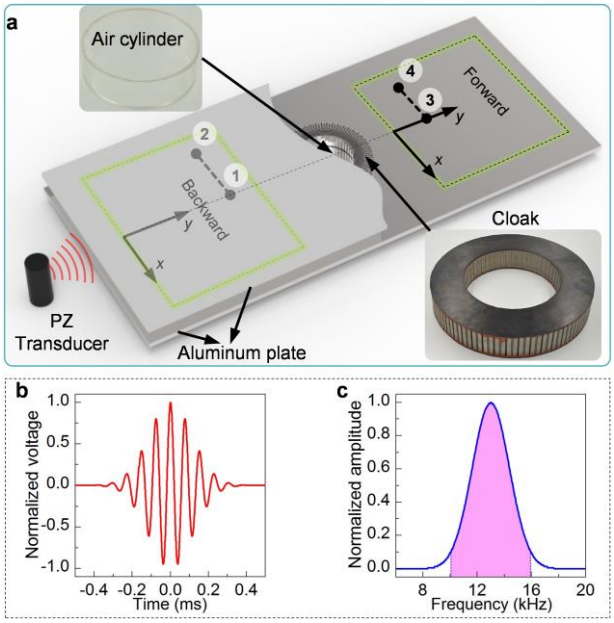

Figure 2 | **Experiment setup for underwater acoustic tests**. **a**, 2D underwater acoustic waveguide composed of two opposing aluminum plates and transducer. Part of the upper plate is removed to show the scatter and cloak position for the experiment. Inset figures show the air cylinder used as scatter and the rubber covered cloak. Forward and backward regions (600 × 560 mm) are 450 mm apart. Locations 1 and 3 lies along the central line of the waveguide and are 475 mm away from the center, while locations 2 and 4 are 200 mm from 1 and 3, respectively. **b, c,** Time and frequency plots of Gaussian burst with central frequency 13kHz and time duration 0.7ms used for driving the transducer.

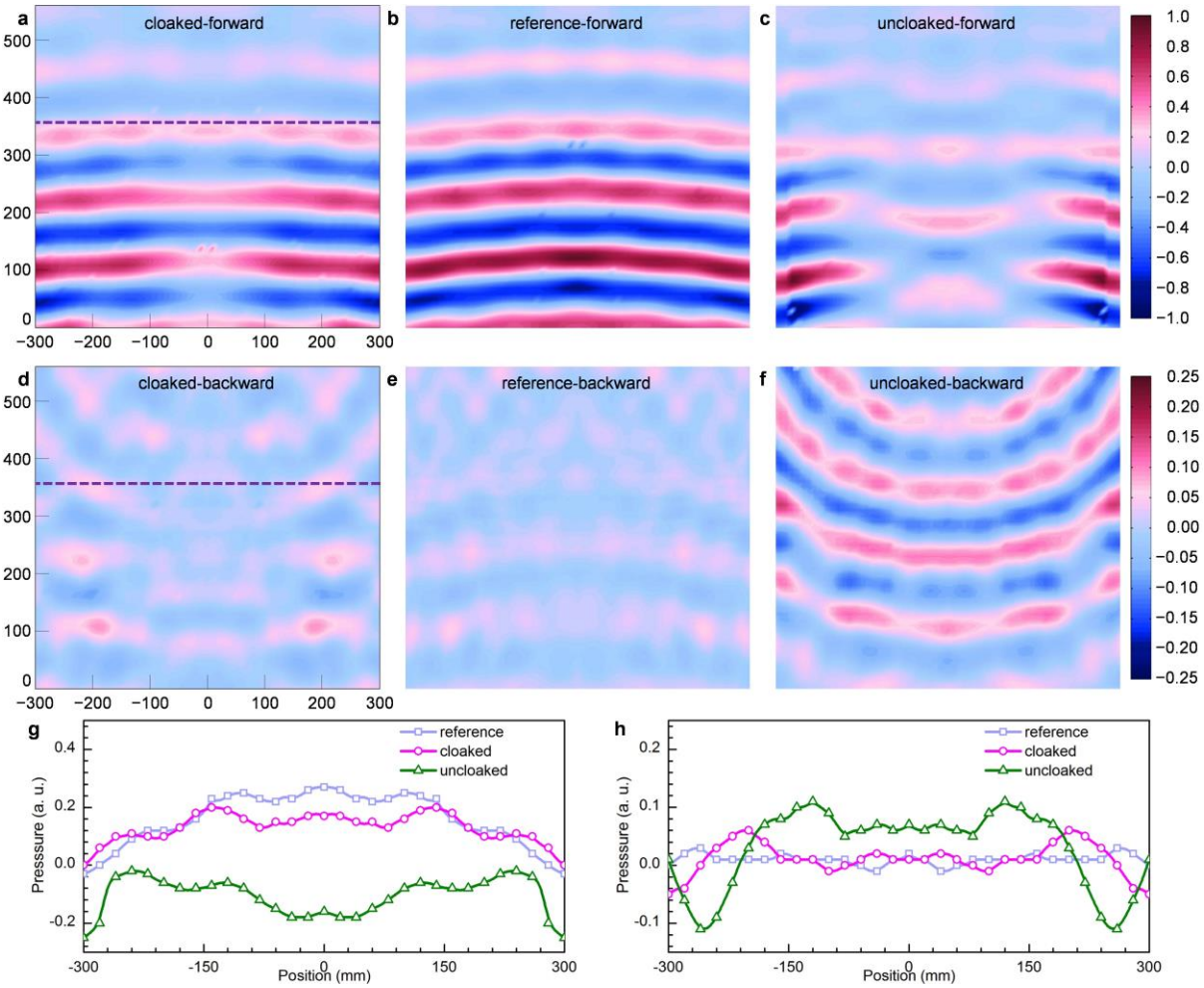

Figure 3 | Measured pressure under incidence of cylindrical Gaussian wave. a, b, c, Instantaneous pressure fields in the forward region for cloaked, reference and uncloaked cases, respectively. **d, e, f,** The same as in **a**–**c** but for the backward region. The cylindrical Gaussian wave is incident from the bottom. Pressure in the forward/backward region was normalized by largest absolute pressure of the reference case in the forward/backward region. Red/blue indicates positive/negative pressure. **g, h,** Pressure distribution for the three cases along the indicated horizontal line y=350 mm in forward and backward regions, respectively.

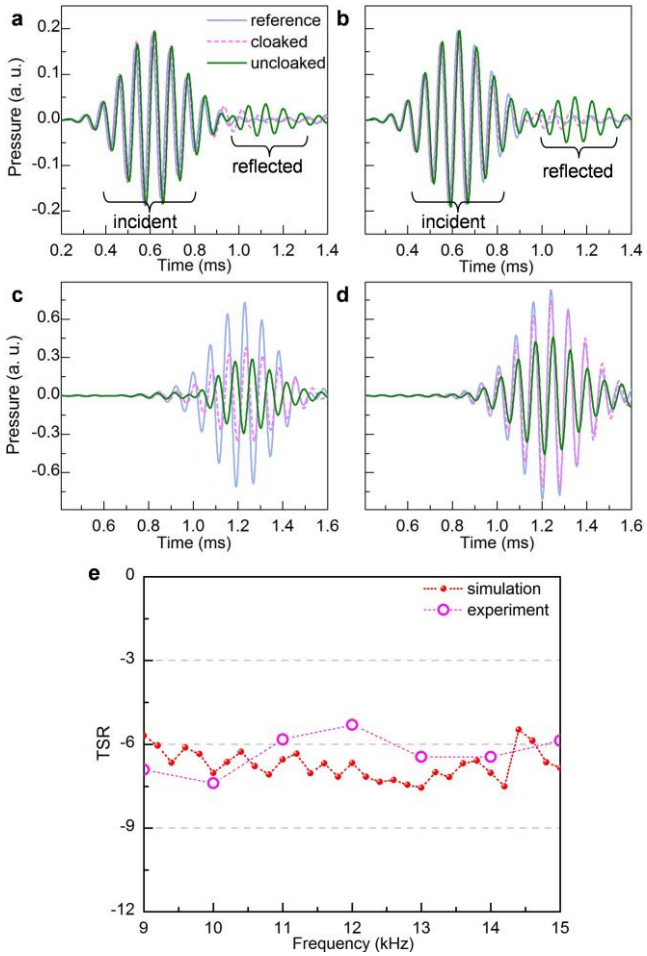

Figure 4 | **Cloaking performance. a, b,** Pressure measured at backward locations 1 and 2 from Fig. 2a. **c, d,** As **a, b** for forward locations 3 and 4 in Fig. 2a. **e,** Simulated and measured cloaked target strength reduction (TSR) for 9–15 kHz.